Journal of Sound and Vibration (2001) **247**(3), 407–416
doi:10.1006/jsvi.2001.3773, available online at http://www.idealibrary.com on IDEAL®

NUMERICAL ANALYSIS OF AERODYNAMIC NOISE RADIATION FROM A HIGH-SPEED TRAIN SURFACE

T. Sassa, T. Sato and S. Yatsui

Nippon Sharyo Ltd, 2-20, *Honohara*, *Toyokawa*, *Aichi* 442-8502 *Japan*.
E-mail: *t-sassa@cm.n-sharyo.co.jp*

(*Received* 21 *February* 2000, *and in final form* 14 *November* 2000)

The aerodynamic noise radiation from a vestibule side door on a high-speed train surface is calculated by the combination of unsteady incompressible fluid flow analysis and acoustic analysis. Pressure fluctuation on a vestibule side door surface is measured to verify the results of fluid flow analysis. Analysis results agree with measured data very well at low frequencies. For high-frequency components, the solvable frequency is limited by the analysis mesh size. Required mesh size is typically one eighth of the wavelength of the pressure fluctuation on the model surface. The aerodynamic noise is mainly radiated from around the following corner where the vortices that are shed from the leading corner strongly interact with the train surface.

1. INTRODUCTION

The aerodynamic noise radiated from a high-speed train causes an environmental problem in Japan, where high-speed railways go through densely populated areas. As the train speed increases, the aerodynamic noise increases roughly as the sixth power of the train speed and the reduction of the aerodynamic noise becomes more important.

In this paper, the noise radiation from a vestibule side door, as an unevenness on a high-speed train surface (Figures 1 and 2), is calculated by the combination of incompressible fluid flow analysis using the finite element method (FEM) and acoustic analysis using the boundary element method (BEM). The results are verified by comparing the measured pressure fluctuation on a vestibule side door with the fluid flow analysis results.

There are few applications of the acoustic analysis to the aerodynamic noise radiation problem from a high-speed train. The objectives of this calculation are to verify the accuracy of our analysis techniques, to understand the mechanism of the aerodynamic noise radiation and to estimate the contribution ratio of the noise radiated from a vestibule side door to the total train noise.

2. ANALYSIS PROCEDURE

Although it is appealing to calculate the aerodynamic noise radiation through a direct solution of a compressible Navier–Stokes equation, it is virtually impossible using exiting computers. The main reasons are as follows:

(1) Sound pressure at an observation point, which is sometimes quite far from a noise source, is much smaller than the pressure fluctuation close to the noise source.

0022-460X/01/430407 + 10 $35.00/0

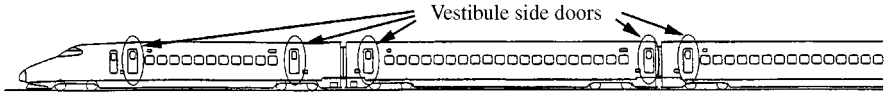

Figure 1. Vestibule side doors of a high-speed train.

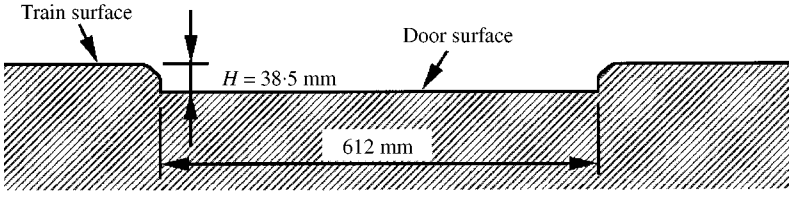

Figure 2. Section of a vestibule.

Therefore, it is very difficult to accurately analyze both the noise source and its propagation simultaneously.

(2) When it is required to calculate the sound pressure level (SPL) at a point far from a noise source, the analysis region must be large and the number of degrees of freedom of the problem becomes very large.

Then, we divide the problem into two sequential parts [1–3]. Namely, we carry out, at first, the unsteady incompressible fluid flow analysis (FEM) of a noise source on a train surface, and second, the acoustic analysis (BEM) of noise propagation from the train surface to far field. We make following assumptions here.

(1) The flow field is not influenced by the acoustic field because the power of the acoustic field is much smaller than that of the flow field.
(2) The fluid flow can be treated as incompressible because the Mach number is small enough in this calculation.
(3) The effect of the motion of the medium on the noise propagation can be neglected because the Mach number is small enough in this calculation.
(4) The dipole noise radiated from a train surface is the principal noise source. The quadrupole noise from the turbulent flow off the surface can be neglected because the Mach number is small enough in this calculation.

3. FLUID FLOW ANALYSIS

3.1. FLUID FLOW ANALYSIS MODEL

Incompressible Navier–Stokes equation,

$$\frac{\partial \mathbf{u}}{\partial t} + (\mathbf{u} \cdot \nabla)\mathbf{u} = -\frac{1}{\rho} \nabla p + v \Delta \mathbf{u}$$

is numerically solved in the region shown in Figure 3. Note that the mesh is refined around the leading and following corners of the vestibule.

The depth H of the step is 38·5 mm, and its width is 612 mm ($\cong 16\,H$). Two-dimensional analysis region is adopted here, ignoring the influence of the header and threshold corners of the vestibule. Also, the mesh has 30 layers in the span direction per 30 mm. The number of nodes is 235 755, and the number of elements is 222 400.

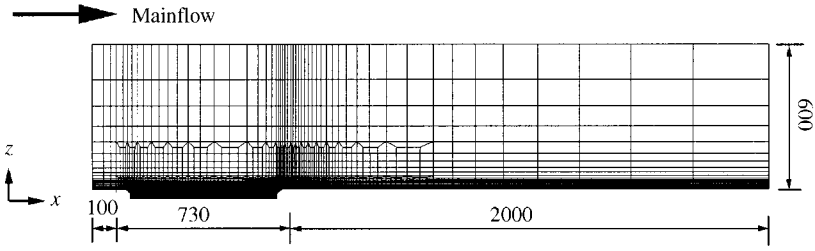

Figure 3. Fluid flow analysis model (section).

The train speed is 75 m/s (270 km/h) and the following inflow boundary conditions are considered.

(1) Time-averaged velocity profile of a well-developed turbulent boundary layer (1/7th power law) at a point 20 m behind the leading nose of a train:

$$\frac{u(z)}{U_\infty} = \left(\frac{z}{\delta_{99}}\right)^{1/7} \quad (z \leqslant \delta_{99}), \qquad \frac{u(z)}{U_\infty} = 1 \quad (z > \delta_{99}).$$

δ_{99} is taken to be 0·61 m (result of another analysis). Note that there is no turbulence in this inflow.

(2) Cyclic symmetry constraint of velocity between the inflow and the outflow, as a demonstration of turbulence in the inflow condition. Unsteady fluid flow analysis is performed on the initial condition of the steady flow pattern under the inflow condition 1.

Smagorinsky's large-eddy simulation (LES) [4] is used to model the effects of turbulence scales smaller than the grid size. The effects of subgrid-scale are considered as the increase of the local viscosity.

$$\nu_{SGS} = (C_S \Delta)^2 \sqrt{2\bar{S}_{ij} \cdot \bar{S}_{ij}}, \quad \text{where } \bar{S}_{ij} = \frac{1}{2}\left(\frac{\partial \bar{u}_i}{\partial x_j} + \frac{\partial \bar{u}_j}{\partial x_i}\right),$$

$\bar{u}_i$ is the grid scale velocity, C_S (= 0·10) is the model constant, and Δ is the grid size defined by the cube root of the element volume.

This calculation was performed using SPECTRUM™ solver in parallel processing on an SGI ORIGIN2000.

3.2. FLUID FLOW ANALYSIS RESULTS

Figure 4 plots the contours of standard deviation in pressure.

In both inflow conditions, the most turbulent regions are (1) where the vortices from the leading corner grow most and (2) where they interact with the following corner.

The velocity profile of inflow condition 2 is shown in Figure 5. The velocity gradient on the wall and the turbulence energy are not so large as those of the well-developed turbulent flow. The power spectrum density (PSD) of the turbulence energy at the point where it is maximum is shown in Figure 6. Comparing with the $-5/3$rd power law of the turbulence energy, inflow condition 2 has larger gradient but has similar global tendency. Namely,

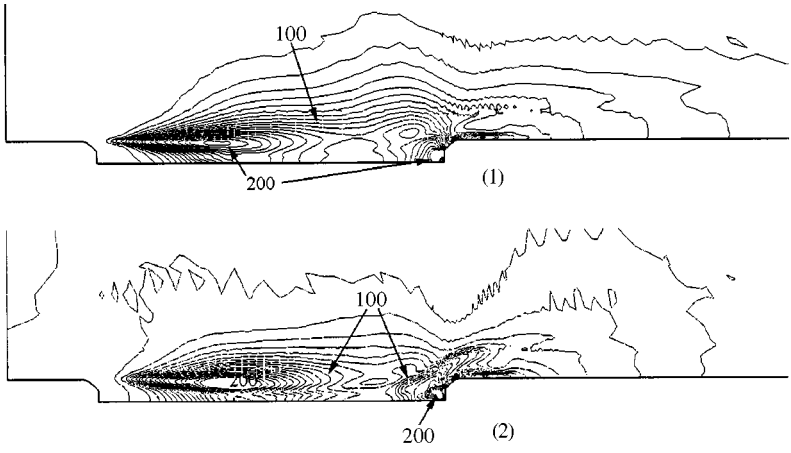

Figure 4. Standard deviation in pressure (0–200 Pa/20 lines): (1) without turbulence in inflow; (2) with turbulence in inflow.

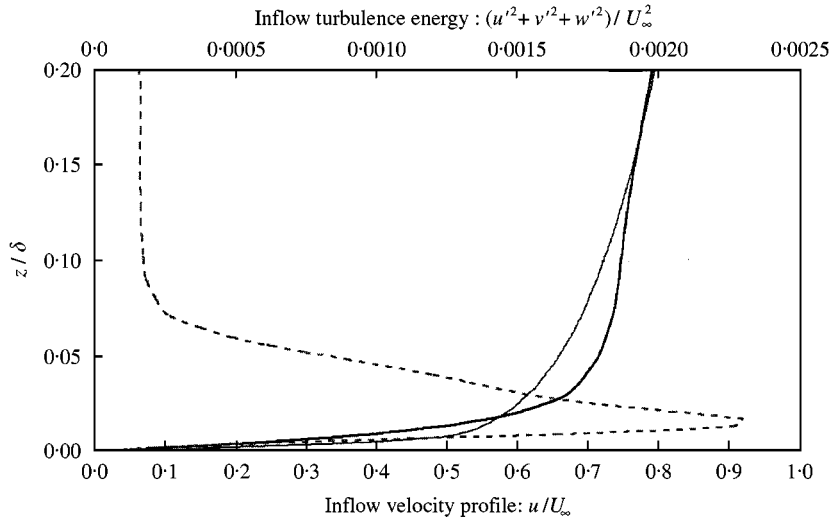

Figure 5. Property of inflow condition 2: ——, 1/7th-power law; ——, velocity profile; – – –, turbulence energy.

inflow condition 2 is a more realistic condition than inflow condition 1, which has zero turbulence energy.

Total wall time for the calculation was typically 300 h for 3000 time steps.

3.3. COMPARISON WITH MEASURED DATA

To verify the results of fluid flow analysis, we made a measurement of pressure fluctuation (pseudo-sound) on a vestibule side door which is located about 20 m behind the leading nose of a high-speed train. Pressure probes were installed close to the following corner where the pressure fluctuation is predicted to be large (Figure 7).

One-third octave band pressure level spectra of analysis results and measured data at two observation points *P*1 and *P*2, which are 53 and 190 mm forward from the following corner, respectively, are shown in Figure 8.

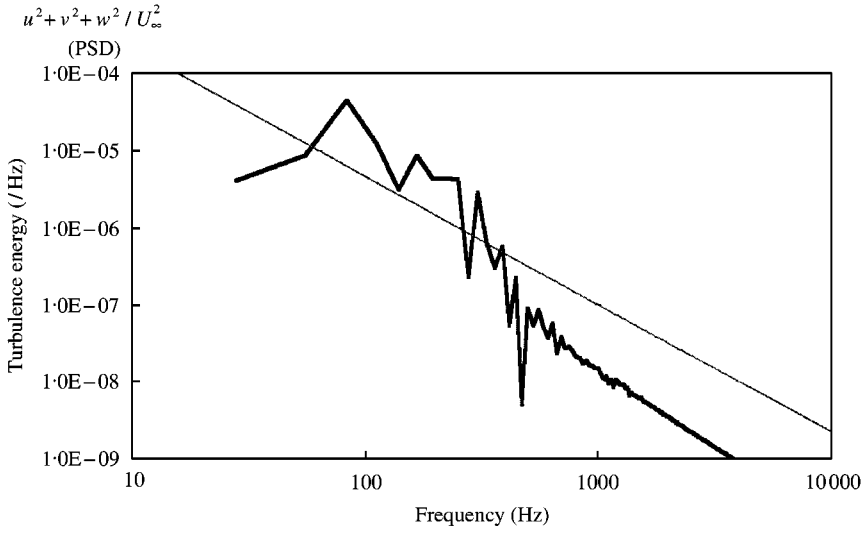

Figure 6. PSD of turbulence energy on inflow condition 2: ——, turbulence energy (PSD); ————, gradient of − 5/3rd-power law.

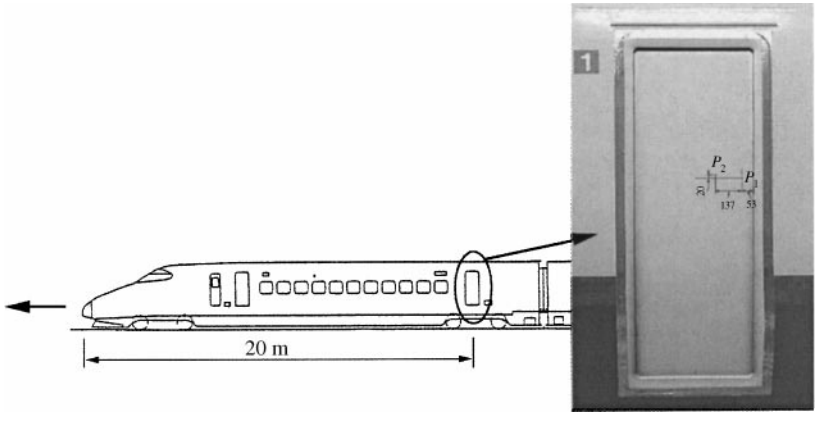

Figure 7. Observation points on a vestibule side door.

From these figures, we observe the following:

(1) Good agreement is obtained between the analysis results and the measured data at low frequencies (lower than 160 Hz).
(2) For high-frequency components (higher than 160 Hz), the analysis tends to underestimate the pressure level. The maximum mesh size on the model surface is about 0·019 m, and the wavelength of the pressure fluctuation at 160 Hz is 25 (m/s)/160 (Hz) ≅ 0·16 m, which is 8 times as long as the mesh size. Here, 25 (m/s) is the phase velocity of the pressure fluctuation (analysis result). In general, it is reasonable that the necessary sampling point density to resolve the moving fluctuation is one-eighth of the wavelength; therefore, the decrease of the pressure level above 160 Hz is caused by the insufficiency of the mesh resolution of this model. A reliable

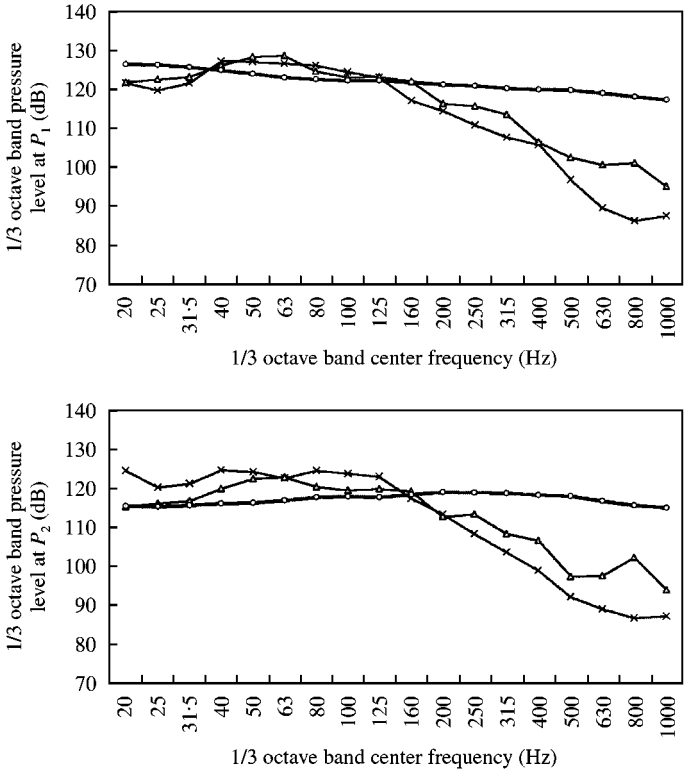

Figure 8. One-third octave band pressure (= pseudo-sound) level on door surface: —×—, analysis without turbulence in inflow (1); —△—, analysis with turbulence in inflow (2); —○—, measurement.

calculation is possible when the mesh size is smaller than one-eighth of the wavelength of the pressure fluctuation.

(3) The high-frequency components are larger in case 2, which has turbulence in the inflow, than they are in case 1. Comparing $P1$ and $P2$, the low-frequency components at $P1$ are much larger than those at $P2$ in the measured data, which agrees with case 2 results. Namely, the airflow is analyzed more realistically with the turbulence in the inflow condition.

4. ACOUSTIC ANALYSIS

4.1. ACOUSTIC ANALYSIS MODEL

The noise propagation problem with time-harmonic load is described by the Helmholtz equation with boundary conditions.

$$\Delta p + k^2 p = 0, \quad \text{with } p = \bar{p} \text{ or } \nabla_n p = \overline{\nabla_n p} \text{ on boundary surface,}$$

where p is the acoustic pressure, k is the wave number defined as $2\pi f/c$ (f is frequency, c is sound velocity), ∇_n is the normal derivative operator and – means given boundary condition value.

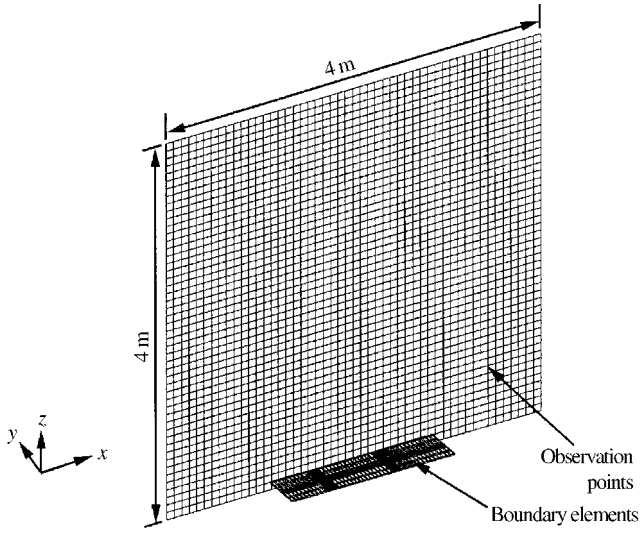

Figure 9. Acoustic analysis model.

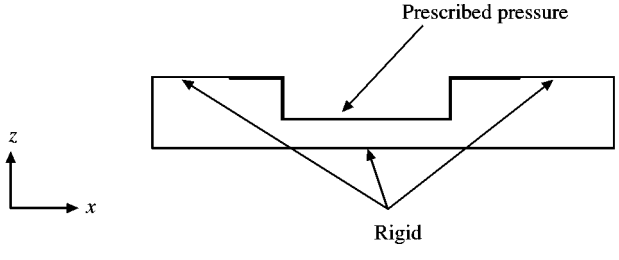

Figure 10. BEM configuration (section).

This problem can be rewritten in the boundary integral equation, which is numerically solved using BEM. SPL at a given observation point can be calculated from the obtained p and $\nabla_n p$ values on boundary surface using the Green function. This calculation is carried out using the RAYON™ acoustic code.

Acoustic analysis model is shown in Figure 9.

We impose the boundary condition of prescribed pressure ($p = \bar{p}$ condition) on the train surface, by applying a discrete Fourier transformation to the pressure fluctuation data of fluid flow analysis (512 timesteps/frame; 4 frames) and removing the monopole component. Around the prescribed pressure elements, rigid elements are placed to expand the train surface and to make the boundary elements closed (Figure 10). Rigid elements have $\nabla_n p = 0$ boundary condition, in which the effects of reflection are considered.

Observation points of sound pressure are provided on a surface shown in Figure 9, and at a point 25 m off the center of a vestibule side door. In order to reduce the statistical errors, the acoustic power of 4 frames is averaged. We assume that the correlation length of turbulence in the span direction is much shorter than the height of a vestibule side door. Then, SPL at the 25 m point radiated from an "entire" vestibule side door can be estimated by multiplying acoustic power by (height of vestibule side door)/(span of analysis region).

These calculations were performed at all FFT frequencies up to 1 kHz.

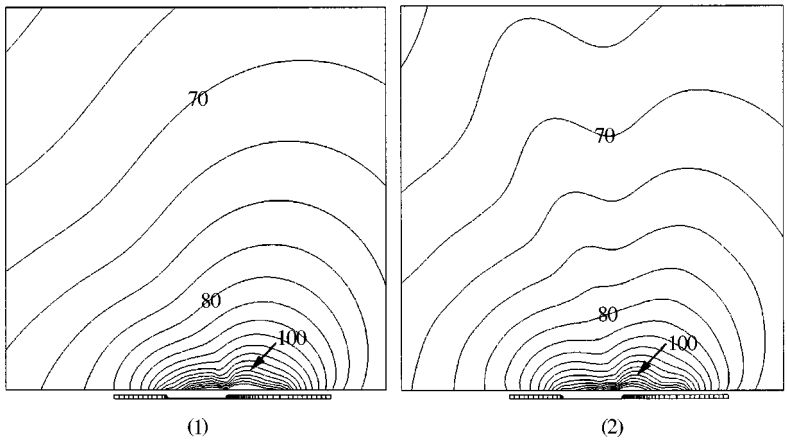

Figure 11. Overall SPL (60–110 dB/20 lines): (1) without turbulence in inflow; (2) with turbulence in inflow.

4.2. ACOUSTIC ANALYSIS RESULTS

Overall SPL distribution (contribution of 30 mm span) is shown in Figure 11, and SPL spectra and overall SPL at the 25 m point (contribution of an entire vestibule side door) is shown in Figure 12 and Table 1. "Overall" means the sum of all 1/3 octave band acoustic power from 20 Hz band to 1 kHz band. The 1/3 octave band SPL is re-calculated from the analysis results at the discrete FFT frequencies.

From these results, we observe the following.

(1) The aerodynamic noise is mainly radiated from around the following corner. Namely, the main noise source is created where the strong vortices that are shed from the leading corner interact with the following corner. Therefore, in order to reduce the aerodynamic noise, it is important to find out the best configuration of the vestibule for reducing the vortex shedding at the leading corner and weakening the vortex interaction with the train surface at the following corner.
(2) In both cases, the low-frequency components are larger than the high-frequency components. The high-frequency components in case 2 are larger than those in case 1. This is the same tendency as is seen in the results of fluid flow analysis.
(3) The decrease of the high-frequency components of SPL at the 25 m point (Figure 12) is smaller than that of the pressure fluctuation on the train surface (Figure 8). This is because the radiation efficiency for the high-frequency components becomes excessively large due to the insufficiency of the mesh resolution.
(4) If we assume that the total train noise at the 25 m point is about 70 dBA, the contribution ratio of a single vestibule side door is several percent. (Note: It is not easy to predict A-weighted overall SPL value accurately, because the solvable frequency is limited by the analysis mesh size.)

5. CONCLUSIONS

We calculate the radiated noise from an unevenness on a high-speed train surface using fluid flow analysis (FEM) and acoustic analysis (BEM). Good agreement is obtained between the fluid flow analysis results and the measured data at low frequencies, which supports the validity of our analysis techniques. However, for high-frequency components,

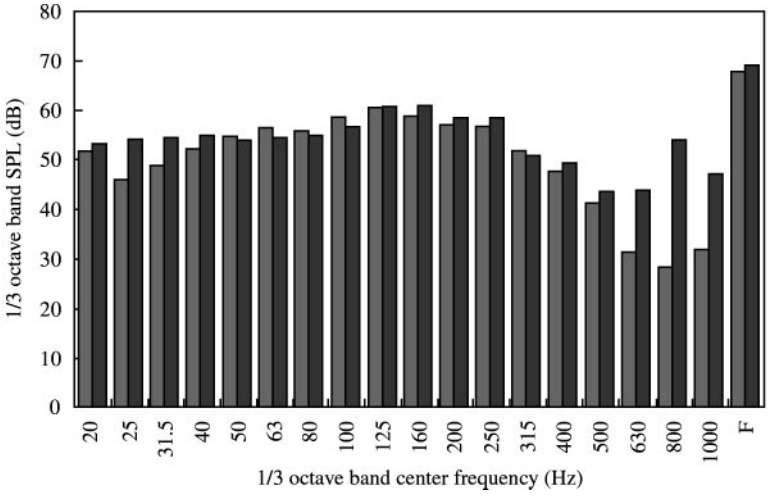

Figure 12. One-third octave band SPL spectra at the 25 m point from an entire vestibule side door: ■, (1) Without turbulence in inflow; ■, (2) With turbulence in inflow.

TABLE 1

Overall SPL at the 25 m point from an entire vestibule side door

	20 Hz–1 kHz overall SPL (dB, dBA)
(1) Without turbulence in inflow	67·1, 53·6
(2) With turbulence in inflow	68·2, 57·3

the analysis tends to underpredict the pressure level because the solvable frequency is limited by the analysis mesh size. We found that the required mesh size in fluid flow analysis is typically one-eighth of the wavelength of the pressure fluctuation on the model surface. We also found that the turbulence in the inflow condition can make a large influence on the flow field. Therefore, to impose a proper inflow condition is very important for a realistic calculation.

The mechanism of the aerodynamic noise radiation is also revealed. The noise is mainly radiated form where the strong vortices that are shed from the leading corner interact with the following corner. This indicates that the proper changes in the configuration of the vestibule may reduce the aerodynamic noise radiation.

The work described above is one of the applications of our analysis techniques to a noise radiation problem. With an increased understanding of both the validity and the limitation of this approach, we can make a contribution to the reduction of the train noise by properly applying our analysis techniques to various noise problems.

ACKNOWLEDGMENTS

We would like to thank Dr Bayard Samuel Holmes, Applied Research Associates Inc., San Francisco U.S.A., who made significant suggestions and comments on this paper.

REFERENCES

1. B. S. HOLMES, J. B. DIAS, B. A. JAROUX, T. SASSA and Y. BAN 1997 *International Journal for Numerical Methods in Fluids* **24**, 1307–1319. Predicting the wind noise from the pantograph cover of a train.
2. M. J. LIGHTHILL 1952 *Proceedings of Royal Society* **211A**, 564–587. On sound generated aerodynamically: I. General theory.
3. N. CURLE 1955 *Proceedings of Royal Society* **231A**, 505–514. The influence of solid boundaries upon aerodynamic sound.
4. J. SMAGORINSKY 1963 *Monthly Weather Review* **91**, 99–164. General circulation experiments with the primitive equations: I. The basic experiment.